Microwave Radiative Transfer through Clouds Composed of Realistically Shaped Ice Crystals. Part II: Remote Sensing of Ice Clouds

K. FRANKLIN EVANS

Program in Atmospheric and Oceanic Sciences, University of Colorado, Boulder, Colorado

GRAEME L. STEPHENS

Department of Atmospheric Science, Colorado State University, Fort Collins, Colorado

(Manuscript received 27 May 1994, in final form 6 December 1994)

ABSTRACT

This paper presents the results of polarized microwave radiative transfer modeling of cirrus clouds containing five different particle shapes and 18 Gamma size distributions. Upwelling brightness temperatures for tropical and midlatitude winter atmospheres are simulated at 85.5, 157, 220, and 340 GHz using scattering properties computed with the discrete dipole approximation (described in Part I).

The key parameter for the results is the sensitivity (ΔT_b/IWP), which relates the modeled brightness temperature depression to the ice water path. It is shown that for the higher frequencies or distributions of larger particles (i.e., in the scattering regime) the sensitivity is nearly independent of cloud temperature and details of the underlying atmosphere. As expected from the single-scattering results, the characteristic particle size has a large effect on the sensitivity, while the distribution width has only a minor effect. The range in sensitivity over the five particle shapes is typically a factor of 2. The sensitivity for a size distribution of solid columns with a median of the third power of the dimension of 250 μm is about 0.1 K/(g m^{-2}). Ratios of ΔT_b's at adjacent frequencies can determine the characteristic size of the distribution, though the relationship is double valued for the most sensitive frequencies considered here. Ratios of ΔT_b at horizontal to vertical polarization contain information about particle shape primarily via the aspect ratio. Ideas concerning the development of a specific cirrus retrieval algorithm are discussed.

1. Introduction

The high altitudes of cirrus clouds, combined with their relatively small optical depths, endows them with radiative properties rather distinct from other types of clouds. The cold temperatures of cirrus clouds mean they emit much less infrared radiation into space than clear skies, thus providing a large "greenhouse" effect (e.g., Stephens and Webster 1981). The reflection of solar radiation by cirrus clouds and the potential surface cooling associated with this reflection is proposed to be fundamental to the evolution of the sea surface temperatures in the tropical western Pacific warm pool (Ramanathan and Collins 1991). Numerical studies have shown that whether cirrus warms or cools the subcloud layer depends on the optical thickness of the cloud (Stephens and Webster 1981; Liou 1986).

Because of their prevalence and radiative significance, it is important that cirrus clouds be accurately represented in climate models. Several types of global measurements of cirrus clouds will be needed to test model predictions. The spatial and temporal distribution of cirrus is needed to confirm GCM output of high cloudiness. The International Satellite Cloud Climatology Project (ISCCP) (Rossow and Schiffer 1991) attempts to provide this type of global distribution by using several geostationary and polar-orbiting satellites that measure clouds with visible and thermal infrared channels. From these two channels the clouds are detected and categorized by cloud top height and optical depth, which are derived using radiative models and a number of assumptions. GCMs are beginning to improve their modeling of clouds by using parameterizations that distinguish cloud water from ice mass in prognostic schemes (Smith 1990; Fowler et al. 1994). Measurements of the ice water content (IWC) of cirrus clouds, which ISCCP cannot provide accurately, are desperately needed for validation of these new cloud modeling parameterizations.

A key element in treating cirrus clouds in climate models is to model their effects on radiative transfer, which is done via parameterization. The development of such parameterizations requires observations of optical and microphysical properties of the clouds. Unfortunately, the optical properties of ice clouds depend

Corresponding author address: K. Franklin Evans, Program in Atmospheric and Oceanic Sciences, University of Colorado, Campus Box 311, Boulder, CO 80309.

on ice crystal shapes and size distributions in ways that are not entirely understood at this time. The high altitude of these clouds makes it difficult to perform in situ measurements of these microphysical quantities, and so they are rather poorly known on a global scale. In addition, the nonspherical shapes of the ice particles has made interpretation of in situ and remotely sensed observations difficult. It is thus desirable to develop remote-sensing techniques that will aid the measurement of cirrus characteristics such as integrated ice mass, characteristic particle size, and particle shape, simultaneously with optical properties such as solar reflectance and infrared emissivity.

Microwave remote sensing offers a number of potential advantages for measuring the ice water path (IWP) of clouds when compared to existing visible and infrared techniques. Visible methods require a number of gross assumptions about ice particle shape, size distribution, and cloud spatial homogeneity to convert from radiance to optical depth to IWP. In addition, thermal infrared techniques require accurate knowledge of cloud temperature. Microwave radiation, to the contrary, interacts with ice particles primarily through scattering, so emission and cloud temperature are relatively unimportant. Since cirrus clouds are above the absorbing part of the atmosphere, they simply modulate the upwelling microwave radiation from below. Furthermore, microwave radiative transfer occurs in the linear regime so the signal is directly proportional to optical depth and cloud spatial inhomogeneity effects are less important. While the effects of particle shape and size distribution are also important for microwave remote sensing of cirrus since they determine the relation between optical depth and IWP, they are more amenable to calculation because the particle sizes are comparable to and smaller than the wavelength. Microwave methods are also complementary to visible and IR methods in that microwave radiation is sensitive to larger ice crystals and to thicker cirrus layers, whereas visible/IR radiation is more sensitive to smaller particles and cirrus clouds of lower IWP.

The purpose of this paper (Part II) is to characterize upwelling microwave brightness temperatures at four frequencies (85.5, 157, 220, and 340 GHz) for cirrus clouds having a range of size distributions and variety of particle shapes. Evans and Stephens (1995, hereafter referred to as Part I) describes the discrete dipole approximation (DDA) scattering computations for the five ice particle shapes and 18 Gamma size distributions considered here. The fundamental effect that cirrus clouds have on upwelling microwave radiation is to decrease the brightness temperature relative to that of the clear atmosphere. It is these resulting brightness temperature depressions that are analyzed for signatures useful for remote sensing IWP and characteristic particle size and shape. A specific algorithm is not proposed as it would necessarily depend on the details of a particular instrument.

The polarized radiative transfer model is described in section 2. Section 3 discusses the modeling setup and tests of the first-order model of Part I. Section 4 presents the results for IWP sensitivities and examines the possibilities for sensing particle size and shape. Some ideas for applying these results to the development of a microwave cirrus remote-sensing algorithm are discussed in section 5, and a summary is provided in section 6.

2. Radiative transfer

Upwelling microwave brightness temperatures from cirrus clouds are computed using a polarized radiative transfer model. There are two important components of the model: one concerns the atmospheric structure and treatment of molecular absorption, and the other solves the polarized radiative transfer equation based on the doubling–adding method. This radiative transfer model requires two types of information about the atmosphere. 1) The microwave scattering properties of ice particle distributions computed by the DDA discussed in Part I. 2) The profile of temperature and gaseous absorption at the specified microwave frequency. In the microwave portion of the spectrum the primary gaseous absorbers in the atmosphere are molecular oxygen and water vapor, and this absorption is computed by the MPM92 (Millimeter-wave Propagation Model 1992) developed by Liebe et al. (1993).

a. The radiative transfer equation

The radiative transfer model used here is a modification of the one described in Evans and Stephens (1991). Whereas that version was for randomly oriented nonspherical particles, the present model treats oriented scatterers. We assume that the ice particles are oriented in the horizontal plane due to aerodynamic forces (see Part I). Since there is no preferred azimuthal orientation, the particle scattering properties depend on the incident zenith angle but not the incident azimuthal angle. The DDA model is used to compute these scattering properties and a discussion of these properties is given in Part I. A more complete description of the DDA and the radiative transfer model is given in a report (Evans and Stephens 1993).

The radiative transfer model solves the monochromatic radiative transfer equation introduced below. The monochromatic equation is appropriate for this study because the particle scattering and atmospheric absorption properties are fairly constant across typical radiometer bandpasses for the window channels considered here. The model also assumes a plane-parallel, or horizontally homogeneous, geometry. In contrast to visible or infrared transfer in clouds, this is a good approximation for computing microwave transfer in cirrus clouds. The small optical depth of cirrus clouds at microwave frequencies means that the spatial inhomo-

geneities present in the clouds are averaged out over the footprint of the sensor. If thermal emission is the only source of radiation in a plane-parallel geometry, then the radiation field is azimuthally symmetric, and of the four Stokes parameters that describe the polarization state of the radiation only I and Q are nonzero. Spatial variability below the cirrus cloud would cause azimuthal asymmetry in the upwelling radiation, but we expect this to have only minor effects. Use of the vertical–horizontal polarization basis is more common in the microwave radiometer field. The two polarization bases are simply related by $I_V = (I + Q)/2$ and $I_H = (I - Q)/2$, where the I Stokes parameter is the total intensity of radiation and Q is proportional to the difference between the vertical and horizontal polarizations.

The Planck function relates the emission from a blackbody to its temperature,

$$B(T) = \frac{c_1}{\lambda^5[\exp(c_2/\lambda T) - 1]},$$

where $B(T)$ has units of W m^{-2} ster^{-1} cm^{-1}, T is the temperature in Kelvin, λ is the wavelength in centimeters, $c_1 = 2hc^2 = 1.1911 \times 10^{-8}$ W m^{-2} sr^{-1} cm^4, and $c_2 = hc/k = 1.4388$ K cm. In the microwave radiative transfer field the Rayleigh–Jeans approximation is often used. This approximation relates the Planck function linearly to temperature, $B(T) \approx c_1 T/(c_2\lambda^4)$, and allows the radiative transfer to be calculated directly in terms of brightness temperature. In this work, however, the Rayleigh–Jeans approximation is not used because of substantial deviations from the Planck function at the high frequencies considered.

After the radiative transfer computation, the I and Q radiances are converted to vertical and horizontal polarizations and expressed in terms of brightness temperatures. There are two ways to convert from a radiance ($I_{\lambda V/H}$) to a brightness temperature. One is to invert the Planck function,

$$T_{\mathrm{EBB}} = \frac{c_2\lambda^{-1}}{\ln[1 + c_1/2\lambda^5 I_{V/H}]},$$

giving the equivalent blackbody temperature. We can compare this temperature to the temperature derived under the Rayleigh–Jeans approximation, namely

$$T_{\mathrm{RJ}} = \frac{2c_2}{c_1}\lambda^4 I_{V/H}.$$

These two different ways of computing the brightness temperature may be related by expressing the equivalent blackbody brightness temperature in terms of the Rayleigh–Jeans brightness temperature as

$$T_{\mathrm{EBB}} \approx T_{\mathrm{RJ}} + \frac{c_2}{2\lambda} - \frac{1}{3}\left(\frac{c_2}{2\lambda}\right)^2 \frac{1}{T_{\mathrm{RJ}}}.$$

This implies that to first order the difference between equivalent blackbody and Rayleigh–Jeans brightness temperature is a constant that depends on λ. For the frequencies considered here this constant offset varies from 2.05 K at 85.5 GHz to 8.21 K at 340 GHz, so the distinction between the two types of brightness temperatures is significant. However, the discrepancy between T_{EBB} and T_{RJ} is insignificant even at 340 GHz when dealing with brightness temperature differences, because the constant offset cancels. Radiometer calibration procedures that assume the Rayleigh–Jeans approximation rely on this offset cancellation. For this work the equivalent blackbody brightness temperatures are used exclusively.

The monochromatic plane-parallel polarized radiative transfer equation with azimuthal symmetry is

$$\mu\frac{d\mathbf{I}(z,\mu)}{dz} = \mathbf{K}(z,\mu)\mathbf{I}(z,\mu) - 2\pi\int_{-1}^{1}\mathbf{M}(z,\mu,\mu')\mathbf{I}(z,\mu')d\mu' - \sigma(z,\mu)B[T(z)], \quad (1)$$

where, $\mathbf{I}$ is the vector of I and Q Stokes parameters, $\mathbf{M}$ is the 2×2 scattering matrix, $\mathbf{K}$ is the 2×2 extinction matrix, σ is the emission vector, $B(T)$ is the Planck function of temperature, z is the height coordinate, and μ is the cosine of the zenith angle ($\mu > 0$ downward).

The scattering matrix $\mathbf{M}$, extinction matrix $\mathbf{K}$, and the emission vector σ for particles are computed using the discrete dipole approximation as described in Part I. These three quantities are related by

$$\mathbf{K}(\mu) = 2\pi\int_{-1}^{1}\mathbf{M}(\mu,\mu')d\mu' + \sigma(\mu),$$

which is a normalization condition that is checked in the DDA code to assure that the discrete angles are adequate to represent the scattering matrix. For a purely gaseous atmosphere, the extinction matrix is diagonal [$\mathbf{K}_{II}(\mu) = \mathbf{K}_{QQ}(\mu) = k_g$], where k_g is the absorption coefficient, the emission vector is unpolarized [$\sigma_I(\mu) = k_g$, $\sigma_Q = 0$], and the scattering matrix is zero. For layers containing both particles and gaseous absorption, the corresponding extinction matrices and emission vectors are added together.

The angular aspects of the radiance field are represented by discrete angles chosen according to Gaussian or Lobatto quadrature schemes. The scattering matrix, extinction matrix, and emission vector are computed by the DDA for a particular set of quadrature angles that the radiative transfer program then uses. For N quadrature angles per hemisphere ($0 < \mu \leq 1$) the radiance field at a particular z level for the $\pm$ (downwelling/upwelling) hemisphere is represented by the vector $\mathbf{I}^{\pm} = (I_1, Q_1, \cdots, I_N, Q_N)$.

b. Adding–doubling polarized model

The doubling and adding method is a relatively standard way of integrating the radiative transfer equation. Since Evans and Stephens (1991) described the application of the doubling–adding model to the solution of (1), only a brief account of the model is presented here. The method requires the atmosphere to be broken down into a number of layers, each with vertically uniform scattering and absorption properties. The temperature structure of a layer is specified by the temperatures at the top and bottom, and a linear gradient in Planck function across the layer is assumed. The doubling–adding method is based on the interaction principle that casts radiative transfer in terms of the reflection $\mathbf{R}$ and transmission $\mathbf{T}$ matrices and source vectors $\mathbf{S}$ for a layer. These properties ($\mathbf{R}$, $\mathbf{T}$, $\mathbf{S}$) of the layer relate the radiation incident upon a layer linearly to the radiation exiting the layer. The matrices are defined for an infinitesimally thin layer of thickness Δz using a discrete finite difference form of (1) leading to

$$|\mathbf{T}^{\pm}|_{iji'j'} = \left[\delta_{ii'}\delta_{jj'} - \frac{\Delta z}{\mu_j}\left(\delta_{jj'}|\mathbf{K}(\pm\mu_j)|_{ii'} - 2\pi w_{j'}|\mathbf{M}(\pm\mu_j, \pm\mu_{j'})|_{ii'}\right)\right]$$

$$|\mathbf{R}^{\pm}|_{iji'j'} = 2\pi\frac{\Delta z}{\mu_j} w_{j'}|\mathbf{M}(\pm\mu_j, \mp\mu_{j'})|_{ii'}$$

$$|\mathbf{S}^{\pm}|_{ij} = \frac{\Delta z}{\mu_j}|\sigma(\pm\mu_j)|_i B(T),$$

where the j are the quadrature angle index, the i are the Stokes parameter index ($i = 1, 2$ for I and Q), the primes indicate incident radiance directions, the μ_j are the quadrature angles and w_j are the quadrature weights, and the δ are Kronecker δ.

From the interaction principle, the properties ($\mathbf{T}$, $\mathbf{R}$, $\mathbf{S}$) of the combination of two adjacent layers can be derived in terms of the individual layer properties. When these layers are vertically homogeneous, that is, when the properties ($\mathbf{T}$, $\mathbf{R}$, $\mathbf{S}$) are the same, the composition rules can be applied repetitively to build up the properties of a layer of any desired thickness. A final layer thickness of δz requires n doubling steps starting from a layer thickness of $\Delta z = 2^{-n}\delta z$. Since it is desirable to have the thermal source (i.e., temperature) vary with depth within a homogeneous layer, we use an extension due to Wiscombe (1976) of the simple doubling formulas for sources that vary linearly with optical depth. If a layer has no scattering, then doubling is bypassed by directly computing the $\mathbf{T}$, $\mathbf{R}$, and $\mathbf{S}$ properties of the layer. The composition formula for two layers with different properties (the adding formula) is used to build up the $\mathbf{T}$, $\mathbf{R}$, and $\mathbf{S}$ properties of the whole atmosphere from the properties of the separate homogeneous layers computed with the doubling formulas.

The surface boundary is treated as a layer with a transmission of unity, the appropriate reflection, and no source term. The radiation emitted from the surface is then the incident radiation on the lower boundary. The model incorporates two types of surfaces: Lambertian and Fresnel. The Lambertian surface emits and reflects isotropic and unpolarized radiation. The Lambertian reflection matrix and emitted radiance vector are

$$|\mathbf{R}_g|_{jij'i'} = 2(1-\epsilon)w_{j'}\mu_{j'}\delta_{i,1}, \quad |I_g^-|_{ji} = \epsilon B(T)\delta_{i,1},$$

where ϵ is the surface emissivity. The Fresnel surface is used to model flat water surfaces at microwave frequencies. The incident radiation is reflected specularly so the incident zenith angle equals the reflected zenith angle. The horizontal polarization is reflected differently than the vertical polarization according to the Fresnel reflection formulas (giving R_H and R_V) for a vacuum–dielectric interface. The Fresnel reflection matrix and emission vector are then

$$|\mathbf{R}_g|_{jj'} = \begin{pmatrix} \frac{1}{2}(|R_V|^2 + |R_H|^2) & \frac{1}{2}(|R_V|^2 - |R_H|^2) \\ \frac{1}{2}(|R_V|^2 - |R_H|^2) & \frac{1}{2}(|R_V|^2 + |R_H|^2) \end{pmatrix}\delta_{jj'},$$

$$|\mathbf{I}_g^-|_j = \begin{pmatrix} 1 - \frac{1}{2}(|R_V|^2 + |R_H|^2) \\ -\frac{1}{2}(|R_V|^2 - |R_H|^2) \end{pmatrix} B(T),$$

where the reflection coefficients are at the angles $\mu = \mu_{j'}$.

This polarized radiative transfer model for oriented particles was tested by comparison to the model for randomly oriented particles for an atmosphere containing spherical ice and water drops and gave identical outgoing brightness temperatures. The radiative transfer model was not specifically tested for oriented particles.

3. Modeling preliminaries

a. Radiative transfer modeling setup

Upwelling polarized microwave intensities are computed for cirrus clouds containing the various particle shapes and size distributions as specified in Part I. To simulate a range of conditions, the cirrus clouds are placed in tropical and midlatitude winter model atmospheres. The tropical (midlatitude) atmosphere has 80% (60%) relative humidity throughout most of the troposphere. The microwave absorption is computed using the MPM92 model of Liebe et al. (1993). Figure 1 shows the profiles of temperature and dewpoint with height for the two model atmospheres, as well as the

transmission to space as a function of height for the four frequencies considered. In the tropical atmosphere only 85 GHz has significant contribution from the surface, while even in the very dry midlatitude winter atmosphere 340 GHz is substantially opaque. This is important for the potential application of these higher-frequency channels to the study of cirrus, as the contribution from the underlying surface, usually highly variable and not well known, is negligible. The transmission approaches unity quickly with height in the lower atmosphere, as a result of the rapid decrease of the atmospheric moisture content with height. So at typical heights of cirrus clouds there is little absorption in and above the clouds at these microwave frequencies.

The polarized plane-parallel multistream model described above is used to simulate the upwelling radiance from cloudy and clear atmospheres. The atmosphere is divided into 20 layers 1.0 km thick that are homogeneous in scattering and absorption properties. The cirrus-cloud layer is 3 km thick and placed at the top of the troposphere [from 9 to 12 km in the midlatitude atmosphere (226–219 K) and from 14 to 17 km in the tropical atmosphere (210–195 K)]. The particle concentration of the clouds and hence the IWC is adjusted for each case so that the nadir brightness temperature depression is 2.0 K for the tropical profile over land. This is done so the change in radiance is small enough to keep the radiative transfer in the linear regime yet large enough so the change in brightness temperature can be accurately computed.

TABLE 1. The ratio of the cosmic background radiation to Planck emission at a typical atmospheric temperature.

Frequency (GHz)	$B(2.7)/B(270)$
Rayleigh–Jeans	0.01000
85.5	0.00429
157.0	0.00185
220.0	0.00081
340.0	0.00015

The radiative transfer simulations are carried out assuming both land and water surfaces because of their marked contrast in microwave radiometric properties. The land is modeled as a Lambertian surface with a constant emissivity of 0.95. The water is modeled as a flat, dielectric, Fresnel reflecting surface with the index of refraction of water varying with frequency and temperature (Ray 1972). The skin temperature of the surface is the same as the bottom of the atmosphere (300 K for tropical and 272 K for midlatitude winter). The cosmic background radiation from above is ignored because at the high microwave frequencies considered here it is insignificant. Table 1 supports this assertion by showing the ratio of the Planck function at 2.7 K to that at 270 K. For the frequencies considered, the 2.7 K blackbody curve departs from the Rayleigh–Jeans

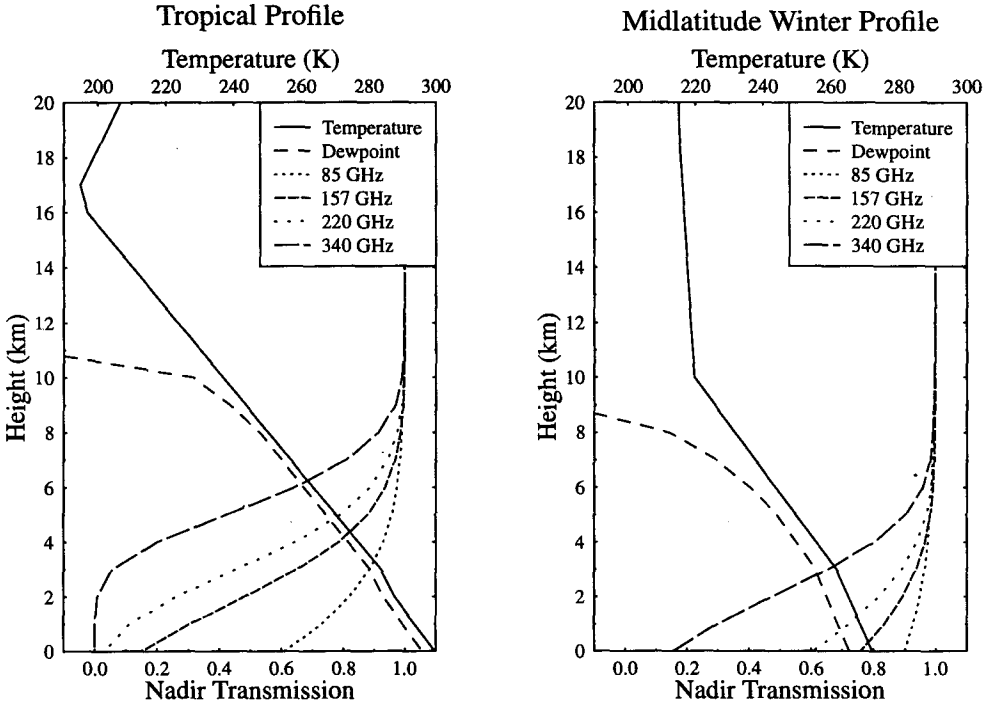

FIG. 1. Temperature, dewpoint, and transmission profiles for the two model atmospheres.

TABLE 2. a) Fractional difference in ΔT_B between FORT and multi-angle results. b) Fractional difference in FORT ΔT_B due to size fitting.

		85 GHz		157 GHz		220 GHz		340 GHz	
a. Atmos.	Surface	rms	max	rms	max	rms	max	rms	max
trop.	land	0.041	0.056	0.016	0.025	0.015	0.024	0.017	0.028
trop.	water	1.227	3.545	0.018	0.031	0.015	0.024	0.017	0.028
midw.	land	0.236	0.456	0.098	0.202	0.053	0.110	0.030	0.045
b.									
trop.	land	0.010	0.035	0.014	0.052	0.020	0.069	0.020	0.069
trop.	water	0.012	0.042	0.014	0.052	0.020	0.069	0.020	0.069
midw.	land	0.011	0.039	0.015	0.058	0.021	0.070	0.021	0.066

limit in such a way as to make it much smaller in terms of actual radiance.

The radiative transfer simulations are performed for four frequencies (85.5, 157, 220, and 340 GHz), five shapes of horizontally oriented particles, (solid columns, hollow columns, hexagonal plates, planar rosettes, and equivalent-volume spheres), and 18 Gamma size distributions $N = aD^{\alpha} \exp[-(\alpha + 3.67)D/D_m]$ (D_m = 70, 100, 150, 250, 400, 700 μm and α = 0, 1, 2). This combination of parameters results in 90 different cirrus-cloud cases for each atmosphere profile and for each surface type (i.e., land and water surfaces). The doubling–adding technique is carried out with eight Lobatto quadrature angles per hemisphere, but results are presented only for the nadir angle (μ = 1) and around 49° (μ = 0.65239).

b. *Test of first-order radiative transfer*

Part I presented a method of fitting the scattering properties as a function of particle size and described a first-order radiative transfer (FORT) model that can be used in conjunction. The scattering fits were presented to give others a quick and simple method of using the DDA results. The FORT model could also provide a basis for a microwave cirrus remote sensing method. The accuracy of the scattering fits and the first-order model are tested by comparing the brightness temperature depressions computed using the fits and the FORT model with the complete DDA scattering information and the multistream radiative transfer model for the cloud/atmosphere scenarios above. The 18 Gamma size distributions are simulated by evaluating the fit equations in Part I and summing over the 13 particle sizes with the appropriate concentrations. There are two sources of error in the fitting/FORT approximation: 1) The error inherent in the first-order radiative transfer model and 2) the error in the fits to the scattering properties. By using the first-order radiative transfer model on the scattering properties with no fitting, the first source of error alone is evaluated, and the two errors can be separated.

The combined errors of the first-order radiative transfer and scattering fits are expressed in terms of the fractional difference in brightness temperature *depression* as compared to the polarized multistream results. The brightness temperature depressions are compared for the three angles/polarizations (0°, 49°V, and 49°H), the 18 size distributions, and the four particle shapes. Table 2a lists the rms and maximum fractional difference for the four frequencies for different combinations of atmospheres and surfaces. At 85 GHz for the tropical atmosphere and frequencies below 340 GHz for the midlatitude winter atmosphere there are significant to very large errors in the first-order model. These errors in the brightness temperature depression are caused by the assumption of no reflection below the cloud. Small amounts of surface reflection can cause large errors in the brightness temperature depression, because there is considerable cancellation between the negative extinction term and the positive emission or scattering terms. There is more cancellation when emission dominates for small particle sizes at the lower frequencies, and so the errors from ignoring reflection are larger in those cases. The effect of surface reflection does not matter when the atmosphere is opaque as it is in the Tropics above 150 GHz or most other places above 300 GHz.

The error due solely to the scattering fits is shown in Table 2b, which lists the fractional ΔT_B differences in the first-order model with and without the fitting. As expected there is little difference between the various atmospheres and surfaces. The typical error goes from about 1% at 85 GHz to 2% at 340 GHz with the maximum error of 7%. At 85 and 157 GHz, the differences are mainly due to the rosette particles' shapes. The fitting procedure for the scattering properties does not add much additional error to the brightness temperature depressions, partly because a size distribution tends to average out the errors at particular particle sizes. The results show that the particle size fits and the first-order radiative transfer model are accurate in most of the situations (higher frequencies/moister atmospheres) relevant to microwave remote sensing of cirrus.

4. Model-derived IWP sensitivities

One advantage of remotely sensing cirrus clouds with microwave radiometry is that the radiative transfer will usually be in the linear regime. This means that the signal (brightness temperature depression) is proportional to the integrated ice mass. Linearity also implies that the signal is affected by the integrated or average properties of the cirrus cloud, so that one need not know the vertical or horizontal distribution of cirrus properties.

When considering the linear radiative transfer regime, a natural quantity to use is the ratio of the brightness temperature depression to the ice water path (ΔT_b/IWP), which here is called the sensitivity. To show the range of linearity, the sensitivity is plotted in Fig. 2 as a function of IWP for a particular simulated cirrus cloud. The IWP includes the secant angle effect for the two angles shown. The sensitivity is independent of IWP in the linear regime, thereafter decreasing with IWP. The useful range of linearity is typically about a factor of 10 in integrated ice mass from the detectability limit (say, $\Delta T_b \approx 3$ K) to where the sensitivity drops by about 10%. The signal still contains useful information beyond the linear regime but is somewhat less convenient to interpret.

a. *Tests of sensitivity invariance*

In section 1 it was claimed that the upwelling microwave radiation from cirrus clouds is independent of cloud temperature and the underlying atmosphere because the cirrus particles are primarily scattering and the clouds are above the significantly absorbing portion of the atmosphere. To test the first assertion, the microwave cirrus sensitivities from a tropical atmosphere over land were compared with cirrus clouds at two different heights. The standard layer of 14–17 km has an average temperature of 201 K, while the other layer of 11–14 km has an average temperature of 220 K. The fractional difference in sensitivity between the two cloud temperature cases is plotted in Fig. 3a. At the higher frequencies only the size distributions dominated by small particles have significant differences in sensitivity. Clouds with smaller particle distributions produce significant emission at the lower frequencies, so that there is a larger dependence of the sensitivity on temperature. In an actual retrieval, the cloud temperature could be estimated more accurately than the 19 K difference used here, and the errors would be correspondingly less.

To test the idea of a decoupling between the cirrus layer and the underlying atmosphere, a comparison was made between sensitivities from the tropical and midlatitude winter atmospheres over a land surface (see Fig. 3b). The average temperature of the cirrus layers in both cases is 220 K. This time the sensitivities are

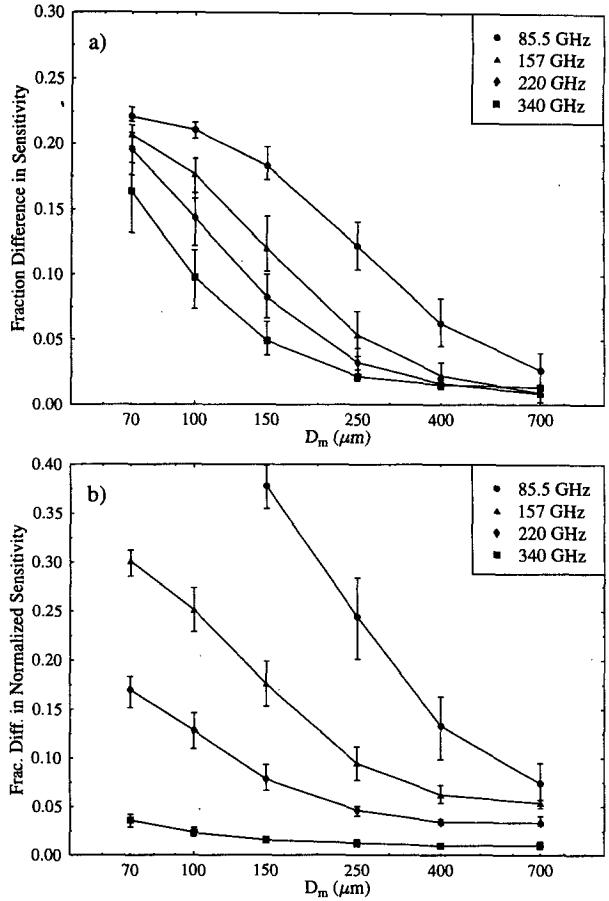

FIG. 3. Fractional difference in sensitivity between a) clouds with average temperatures of 201 and 220 K in a tropical atmosphere, and b) clouds with same average temperature of 220 K but different patterns of incident radiation from tropical and midlatitude winter atmospheres. The error bars show the range over the five particle shapes.

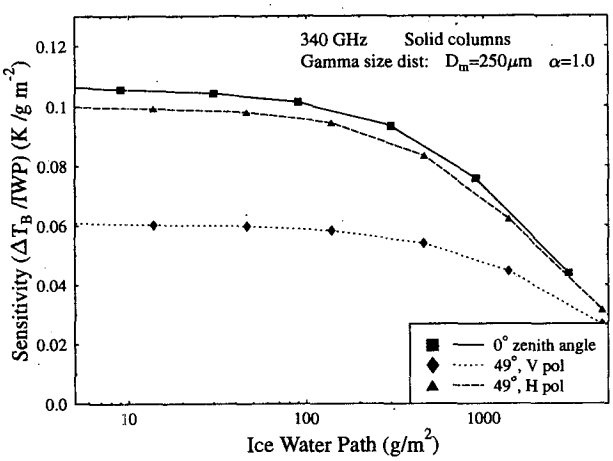

FIG. 2. Sensitivity vs IWP showing the range of radiative transfer linearity.

normalized by the upwelling brightness temperature $[\Delta T_b/(\text{IWP } T_b)]$. The normalized sensitivities for the two atmospheres are within 10% for 340 GHz and all but the two smallest size distributions at 220 GHz. The smaller size distributions and lower frequencies have considerable differences in sensitivity. This results from the high amount of emission, which is not proportional to the upwelling brightness temperature as is scattering. In fact, for the midlatitude winter atmosphere over a water surface the sensitivities of some of the smaller size distributions at 85 and 157 GHz are actually negative (the cirrus cloud causes a rise in brightness temperature), because the cloud is warmer than the brightness temperature of the radiation emitted from the surface. Again, in actual practice the structure of the underlying atmosphere would be better known than the difference between the two profiles in this comparison.

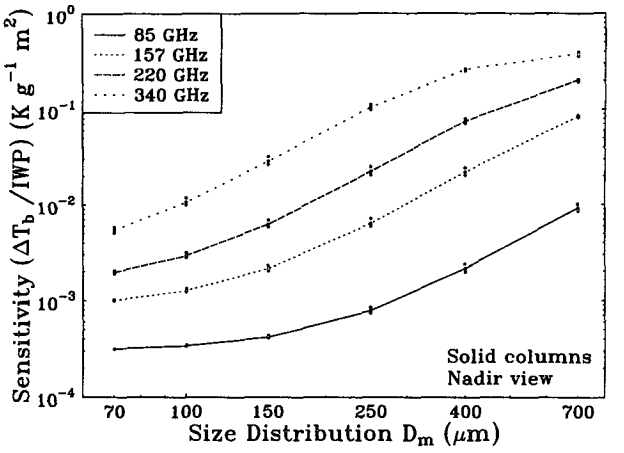

FIG. 4. Nadir-view sensitivity as a function of size distribution for solid columns. The three size distribution widths (α = 0, 1, 2) for each D_m and particle shape are shown as dots.

b. Sensitivity and particle size

The results presented below show how sensitivity (ΔT_b/IWP) depends most strongly on the frequency of the radiation and on the Gamma size distribution parameter D_m (the median of the third power of the particle size). Figure 4 shows the sensitivity for solid columns for the 18 size distributions and four frequencies. Cirrus clouds composed of particles defined by size distributions with large particles ($D_m \geq 400$ μm) produce higher sensitivities (more than a factor of 10) compared to clouds composed of smaller particles ($D_m \leq 100$ μm). The effect of the Gamma size distribution parameter α (related to the width of the distribution) is much less pronounced (note the three vertically aligned dots at each D_m). For the tropical atmosphere above a land surface, the sensitivity varies on average 7% and at most 20% over α = 0, 1, 2 for all angles, particle shapes, and size distributions. This implies that the gamma distribution parameter D_m characterizes the "average" size of the distribution rather well.

One problem with passive microwave remote sensing of cirrus is that, depending on the maximum frequency of observation, much of the cirrus cloudiness may be too thin to detect. If the geometric limit for extinction in the visible is used, then the optical depth can be related to the integrated IWP by

$$\tau = 2\frac{\langle A\rangle}{\langle V\rangle}\frac{\text{IWP}}{\rho_i},$$

where $\langle A\rangle$ is the projected particle area averaged over the size distribution, $\langle V\rangle$ is the average volume, and ρ_i is the density of ice (Table 4 in Part I lists $\langle V\rangle/\langle A\rangle$ for the distributions). For solid columns with the aspect ratios used here and a Gamma distribution with α = 1 the visible optical depth is approximately related to the D_m parameter by $\tau \approx 10(\text{IWP})/D_m$, where the IWP is in g m^{-2} and D_m is in μm. Cirrus as thin as τ = 0.03 is detectable visually from the ground (Sassen and Cho 1992). For a given IWP, larger particle sizes cause a reduction in the visible signal but a dramatic increase in the microwave signal. A minimum detectable cirrus IWP can be defined by the IWP required to give a brightness temperature depression of 3 K. Figure 5 shows the minimum detectable IWP for nadir viewing with a tropical atmosphere over a land surface. For example, at 340-GHz solid columns with D_m = 250 μm an IWP of 30 g m^{-2} gives a ΔT_b = 3 K, so a 3-km thick cirrus layer with an IWC of 0.01 g m^{-3} would be detectable. At the maximum frequency considered here (340 GHz) the thicker cirrus clouds, especially with larger particles, would be detectable but much visible cirrus would not.

Given the wide range in sensitivities for different particle distributions, it is important to have some method to infer these cirrus properties so that the integrated ice mass can be retrieved uniquely. For passive microwave radiometry the potential observables are brightness temperatures at different frequencies, for vertical and horizontal polarizations, and perhaps at different angles. One way to use the additional information from multiple channels is to take ratios of brightness temperature depressions, which are equivalent to ratios of sensitivities if the observations are in the linear radiative transfer regime so that the IWP drops out. In the following, the sensitivities for the tropical atmosphere over a land surface are used.

Ratios of brightness temperature depressions at different frequencies provide information about the characteristic particle sizes in cirrus. Figure 6 has plots of sensitivity as a function of ΔT_b frequency ratio for three frequencies. The six different size distribution parameters D_m are plotted with different symbols, so the progression of characteristic size along the curves can be seen clearly. Unfortunately, for the frequencies with useful sensitivities (220 and 340 GHz) the relationship

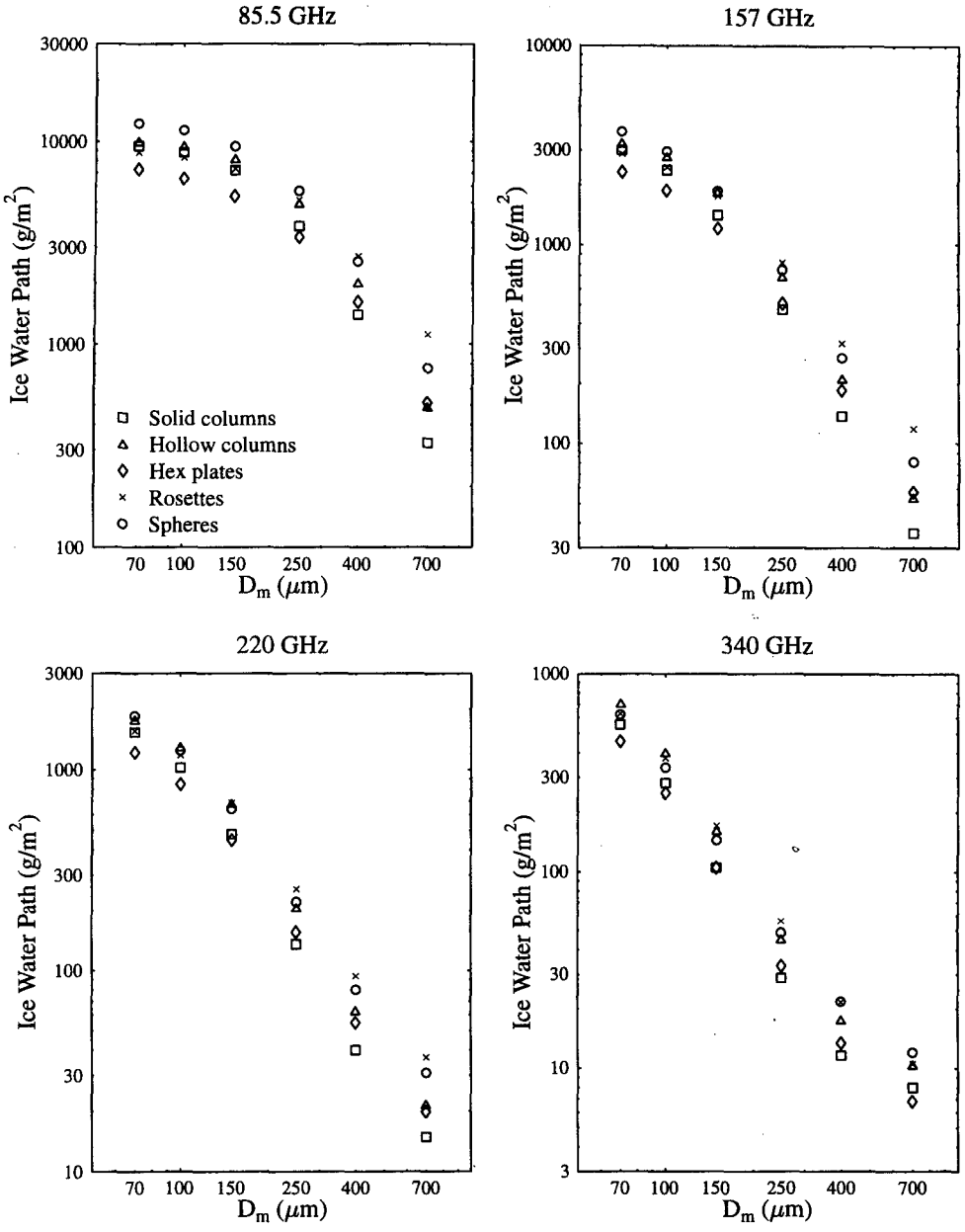

FIG. 5. Minimum detectable cirrus IWP for $\Delta T_b = 3$ K at a nadir view. Only the $\alpha = 1$ distributions are plotted.

between sensitivity and ΔT_b frequency ratio is multivalued, with one branch having size distributions below about $D_m = 250$ μm and the other branch having the larger sizes. If it is known a priori that the particle sizes are in the upper part of the range, then one may be able to use just the upper part of sensitivity versus ΔT_b frequency ratio curve. Thus, some additional information about the particle sizes is needed at these frequencies.

One might think that it would help to use two or more ΔT_b frequency ratios instead of one, but there is a limit to how much information can be extracted from multiple frequencies. Because the scattering properties of ice vary smoothly in the microwave (no absorption bands), frequencies must be well separated to give distinct information. On the other hand, frequencies that are very widely separated (more than a factor of two) will have such divergent sensitivities that the cirrus will not be detectable with the lower frequency (this is certainly true if the higher frequency is still in the linear regime, $\Delta T_b <$ 30 K). For this reason it is probable that only one frequency ratio will be useful.

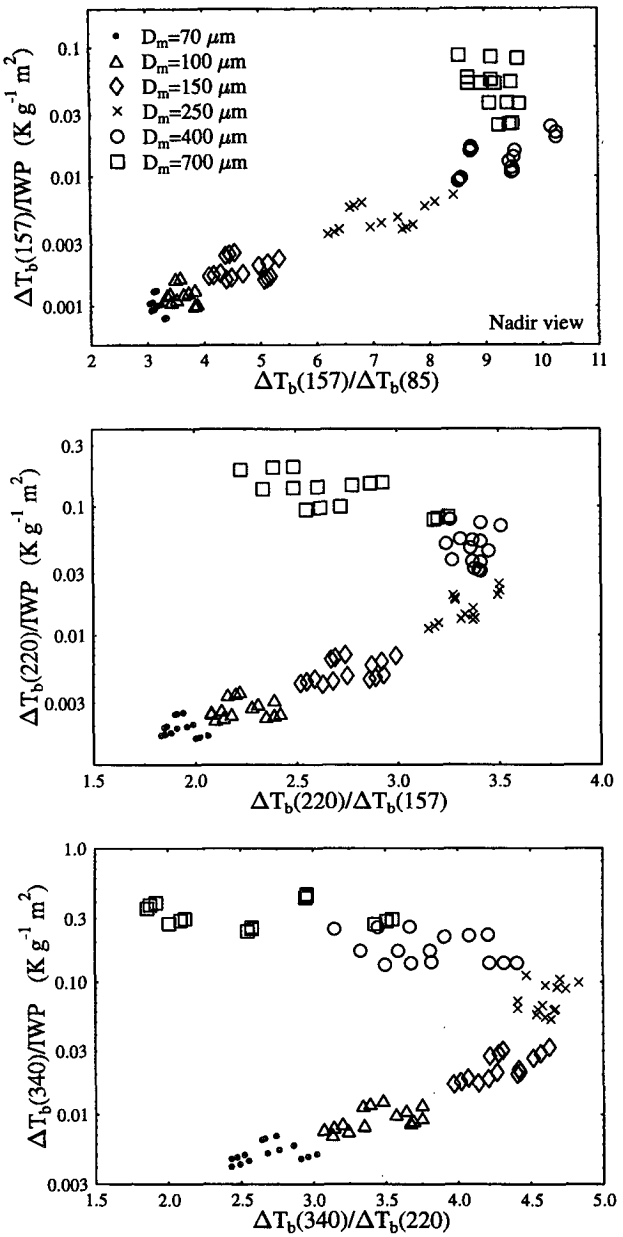

FIG. 6. Sensitivity vs ratio of ΔT_b at different frequencies. The sensitivity is shown for three frequencies at a nadir view angle. Plotted on each graph are the five shapes and 18 size distributions, with the six different size distribution parameters D_m shown by symbols.

We might expect that if even higher frequencies were used, then most of the size distributions would end up on the upper part of the curve, thus lessening the multivalued problem. To test this idea, scattering and radiative transfer calculations were carried out at 460 GHz for the spherical particles only. The same particle densities, size distributions, and radiative transfer procedures described above were used. Figure 7 shows sensitivity versus ΔT_b frequency ratios for 220, 340, and 460 GHz for all the size distributions of spheres. The 460 to 340 GHz ΔT_b ratio plot has only the two smallest size distributions on the lower branch of the curve. We expect that even higher frequencies would be completely single valued. Another advantage of higher frequencies is that the sensitivities, besides increasing and lowering the IWP detectability limit, increase more slowly with particle size. This means that less accuracy is needed in knowing the characteristic

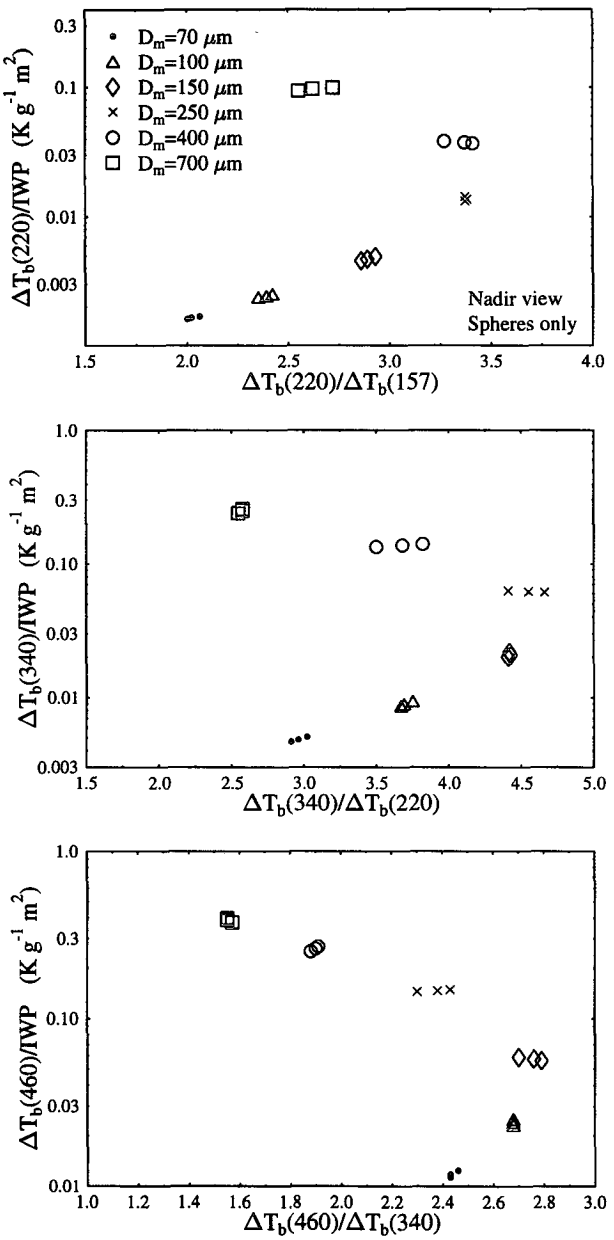

FIG. 7. Sensitivity vs ratio of ΔT_b at different frequencies. The sensitivity is shown only for spheres for 220, 340, and 460 GHz at a nadir view angle. Plotted on each graph are the 18 size distributions, with the six different size distribution parameters D_m shown by symbols.

size of the particles in order to have acceptable accuracy in the retrieved ice mass. Thus, there appears to be much to gain in cirrus remote sensing from radiometers in the submillimeter portion of the spectrum.

Besides the limitations of instrumentation, we can identify an approximate limit to how far up in frequency one can go and still have the same microwave-scattering behavior. The imaginary part of the index of refraction of ice, which governs absorption, increases rapidly in the THz (10^{12} Hz) region, so that cirrus clouds would leave the scattering regime and enter the absorption regime and behave as they do in the infrared. For the spherical particles at −60°C with a Gamma distribution $D_m = 400$ μm, the single scattering albedo drops to 0.90 at 1260 GHz. The water vapor absorption also increases with frequency so that there will be significant emission from the atmosphere in and above the cirrus clouds.

c. *Sensitivity and particle shape*

The range in sensitivity over the various particles shapes is smaller than for particle size but still significant. For the tropical atmosphere, the range in sensitivity over the five shapes is a factor of 1.9 on average and a maximum of 4 for all angles and size distributions. As an example, Fig. 8 shows the sensitivity at 340 GHz for the 18 size distributions and five particle shapes. For 340 GHz and nadir view angle the maximum range is only a factor of 2.0. Given the range of sensitivity due to particle shape it is desirable to be able to infer some information about shape from the microwave radiometry observables.

The ratio of brightness temperature depressions for the two polarizations (horizontal over vertical) contains information about cirrus particle shapes. Figure 9 has plots of sensitivity as a function of ΔT_b polarization ratio for 220 and 340 GHz, with the shapes plotted as different symbols. The major contributing factor for the sensitivity is the size distribution parameter D_m, rather than the shape, so the six size distributions for each shape tend to be aligned along the sensitivity axis. The ΔT_b polarization ratio separates the particles shapes according to the aspect ratio, from the spheres with a ratio of 1.0 to the plates with a ratio from 1.7 to as much as 4.0. There is a tendency for the ΔT_b polarization ratio to increase with characteristic particle size, mainly because of the decreasing aspect ratio. For columns at 340 GHz, the ΔT_b polarization ratio decreases for distributions with the largest particles, because of the non-Rayleigh scattering effect. With information about the characteristic size of the distributions, it looks possible to use the ΔT_b polarization ratio to determine a distribution of particle shapes. Actual bullet rosettes complicate the picture greatly. Because of the presumably random attachment of bullets, they should have a polarization ratio between that for spheres and for planar rosettes.

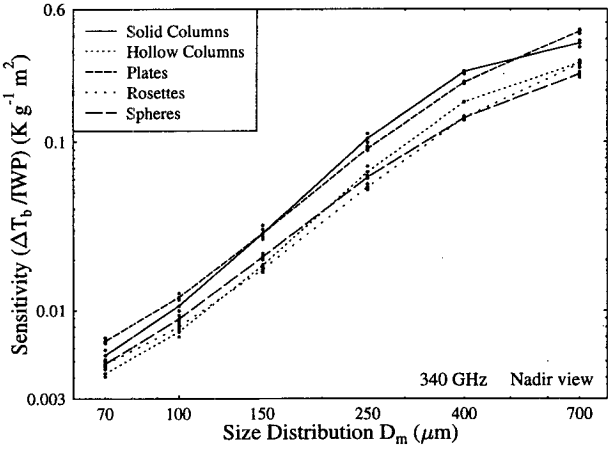

FIG. 8. Nadir-view sensitivity as a function of size distribution for 340 GHz for the five particle shapes.

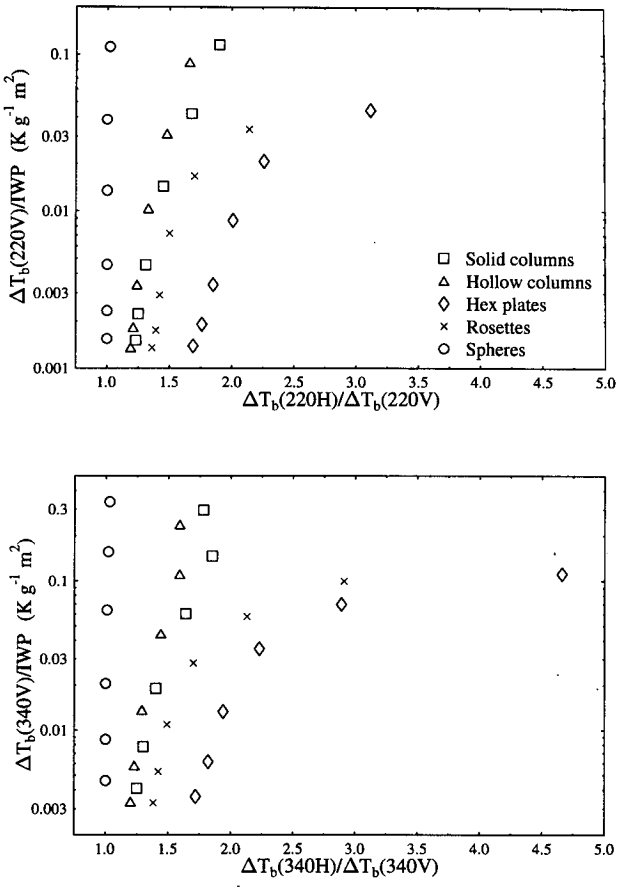

FIG. 9. Sensitivity vs ratio of ΔT_b for horizontal polarization to that for vertical polarization at 49°. The sensitivity is shown for 220 and 340 GHz. Plotted on each graph are the six size distributions with $\alpha = 1$ and the five particle shapes, with the different shapes shown by symbols.

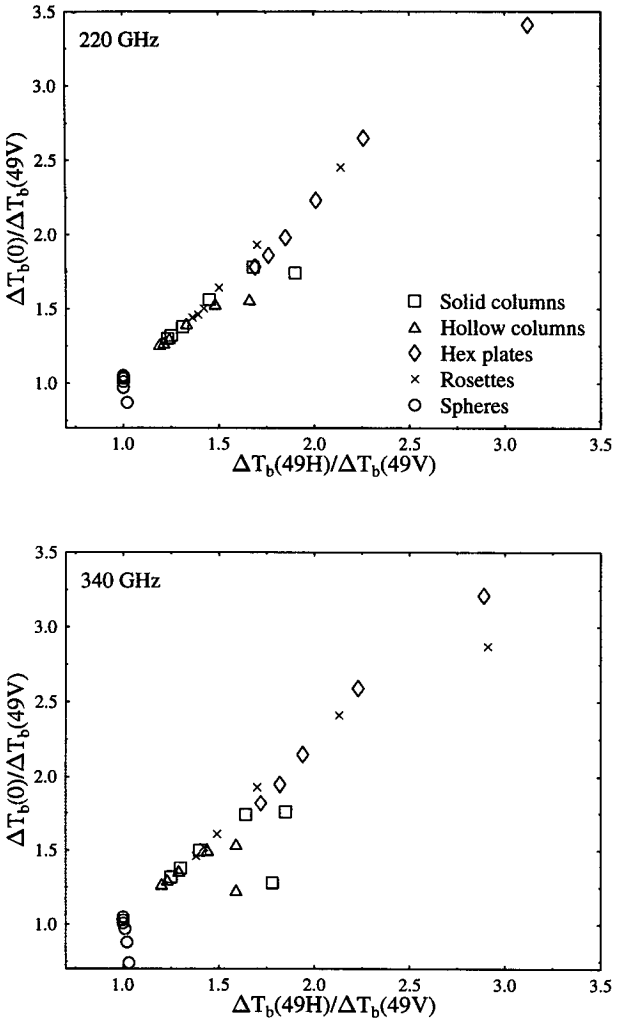

FIG. 10. Ratio of ΔT_b for 0° to that for 49° vs ratio of ΔT_b for horizontal polarization to that for vertical polarization at 49°.

The ratio of brightness temperature depressions at two angles (0°, 49°) has information much like that from the polarization ratio. Figure 10 shows the angular ΔT_b ratio versus the ΔT_b polarization ratio for 220 and 340 GHz. The plot is close to a straight line (except for the large particle distributions at 340 GHz), indicating that the information from the angular pattern of the brightness temperature depression is almost equivalent to the polarization information. It is generally much easier to measure the two polarizations at a fixed angle than to measure the same cloud volume at two angles, so there is probably little point in trying to use the angular pattern of radiation for microwave remote sensing of cirrus.

Part of the effect of shape on sensitivity is due to the aspect ratio, but part is also due to the particle volume. The planar rosettes, for example, have less volume than the columns for the same maximum particle extent D. Even though the concentration is normalized to have the same IWC, this means that the rosettes have a smaller "effective" size. To examine this particle volume effect Fig. 11a plots the 340-GHz sensitivity at a nadir viewing angle against a characteristic size based on the equivalent-volume sphere diameter. This characteristic size is $\langle D_{eq}^6 \rangle^{1/6}$, which is proportional to the Rayleigh scattering cross section. Using the characteristic size spreads the shapes out across the size axis but does not give a tighter sensitivity relationship (compare with Fig. 8). The columns and rosettes fall on a smooth curve, but the plates and spheres are above and below. At nadir the plates have relatively more scattering for their volume, while the spheres have relatively less. Figure 11b shows the same plot but for vertical polarization at 49°. For vertical polarization at this angle, there is a much tighter relationship between sensitivity and particle volume characteristic size. To quantify this the sensitivity for the four middle size distributions is

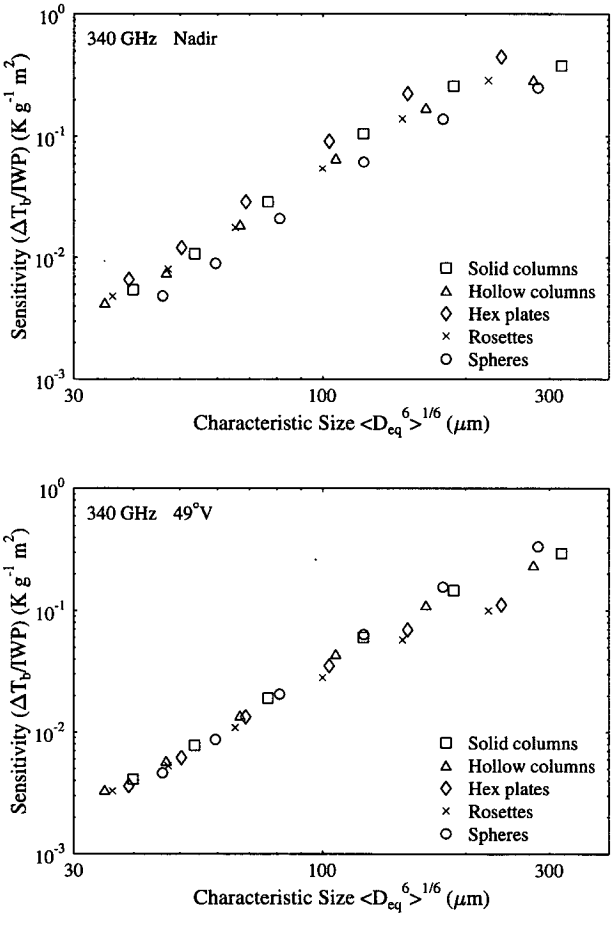

FIG. 11. Nadir view (a) and 49° vertical polarization (b) sensitivity at 340 GHz vs a characteristic particle size of the distributions. This characteristic size is the sixth root of the sixth moment of the equivalent-volume diameter. The $\alpha = 1$ distributions are plotted for the five shapes.

fit (linearly in the logs) against the characteristic size. For nadir angle and horizontal polarization at 49°, the rms error is about 0.24 for the characteristic size, based on particle volume or on the maximum particle size. For vertical polarization at 49°, however, the rms error is 0.30 for the maximum particle dimension fit and only 0.13 for the volume-based characteristic size fit. So there appear to be certain angles and polarizations that minimize the confounding effects of particle shape if the particle volume is taken into account when assigning a "characteristic size" to the size distribution.

Particle shape is mostly important as it affects the sensitivity and hence the retrieval of IWP. If ΔT_b polarization and frequency ratios can uniquely determine the sensitivity, then the effect of shape can be dealt with through the polarization information without specifically finding the shape. This idea was investigated by determining how the sensitivity varies with the ΔT_b frequency and polarization ratios. It was found that there is still ambiguity in the sensitivity due to shape that the ΔT_b polarization ratio does not resolve.

5. Implications for a cirrus retrieval scheme

The details of a cirrus microwave remote-sensing algorithm will depend on the particular instrument in question, which establishes the frequency and polarization capabilities as well as the experimental setup. Since high-frequency microwave observations of cirrus are just becoming available,[1] a specific algorithm is not proposed. Instead general concepts will be discussed that should aid in applying the numerical results above to develop a future retrieval algorithm.

Since the basic signal relating to the mass of cirrus is the brightness temperature depression (i.e., the difference between the brightness temperature of the clear sky minus that over the cirrus cloud), as with many cloud detection and measurement methods, knowledge of the clear-sky brightness temperature is required. An obvious method of obtaining the clear-sky brightness temperature is to use nearby pixels having no or very thin cirrus. This requires the assumption that the atmosphere beneath the cirrus layer is horizontally homogeneous. In atmospheres having at least a modest amount of water vapor the higher microwave frequencies (say, >200 GHz) are effectively opaque to the surface. Thus, possible subcirrus inhomogeneities would be caused by water vapor irregularities and lower water clouds. The lower microwave frequencies that are insensitive to cirrus could be used to correct for water vapor, and potentially even lower cloud, irregularities. Water vapor profiling channels such as ones at 183 GHz may help in correcting for humidity irregularities, though these channels would also be modified by scattering in cirrus clouds.

Once brightness temperature depressions (ΔT_b) have been computed, the procedure for determining the IWP rests on determining the correct sensitivity (ΔT_b/IWP). This assumes that radiative transfer is in the linear regime, which would usually be the case. A more general (and complicated) method would use a radiative transfer model that operates on tabulated scattering properties to iteratively find a solution satisfying the observables. To determine the correct sensitivity one must know, first, the characteristic particle size, and second, the particle shape. In situations with a mixture of particle shapes some idea of the shape mixing fractions is needed. The characteristic particle size can be estimated from ΔT_b ratios at different frequencies (see Fig. 6). If there is uncertainty about which branch of the curve to use, or if the ΔT_b at the highest frequency is too low for a ΔT_b frequency ratio to be measurable, then a characteristic size would have to be assumed. This could come from successfully found sizes in adjacent pixels, crude sizes based on parameterizations using cloud temperature, or effective radius retrievals using information from other spectral regions such as infrared wavelengths. If polarization information (horizontal and vertical channels) is available, then that can be used to help determine particle shape using the ratio of ΔT_b at the two polarizations (see Fig. 9). There is some ambiguity in the relationship between particle shape and ΔT_b polarization ratio, so extra information would be useful. If no polarization information is available, then it may be best to assume a crystal habit based on environmental conditions (e.g., columns in coldest clouds, bullet rosettes in more convective regimes, plates in warmer clouds).

It would be best to use collocated visible and infrared channels in conjunction with the microwave frequencies to measure cirrus properties. First of all, the visible and thermal IR channels could be used to detect the presence of cirrus. Since the microwave channels are only able to detect moderate to large optical depths, the cirrus emissivities will be fairly large and a good estimate of cloud-top temperature could be made. The cloud temperature can be used to aid in the selection of ice crystal habit and perhaps particle size. Several near infrared channels (e.g., Wielicki et al. 1990) or thermal infrared channels (e.g., Parol et al. 1991) or both types (e.g., Ou et al. 1993) can be combined to estimate effective radius.

6. Summary and conclusions

In an effort to learn about the issues important for microwave remote sensing of cirrus, brightness temperatures at 85.5, 157, 220, and 340 GHz were computed for cirrus clouds composed of various shapes and size distributions of ice particles. The scattering prop-

[1] The Millimeter-Wave Imaging Radiometer (MIR) in a preliminary configuration was flown during the Tropical Oceans Global Atmosphere Coupled Ocean–Atmosphere Response Experiment (TOGA COARE) (see section 6).

erties for Gamma size distributions of horizontally oriented solid columns, hollow columns, hexagonal plates, planar four bullet rosettes, and equivalent-volume spheres were computed with the discrete dipole approximation (see Part I). The radiative transfer calculations were carried out with a fully-polarized plane-parallel doubling–adding model assuming azimuthal symmetry. The Rayleigh–Jeans assumption was not used in light of the high frequencies considered.

Standard tropical and midlatitude winter atmospheres were used in the simulations. In the tropical atmosphere there is little or no transmission from the surface for the three higher frequencies. At typical heights of cirrus clouds and above there is virtually no gaseous emission at these frequencies. The radiative transfer simulations are done for 3-km thick clouds at appropriate heights over land and water surfaces. The brightness temperatures at nadir and near 49° are used in the analysis. Since cirrus clouds at microwave wavelengths will usually be in the linear radiative transfer regime, a natural quantity to consider is the ratio of the brightness temperature depression to ice water path (ΔT_b/IWP), which here is called the sensitivity.

The range of linearity is about a factor of 10 from a detectable limit of a brightness temperature depression of 3 K to around 30 K. A test with cirrus clouds at different heights in the tropical atmosphere shows that the sensitivity is independent of temperature except for the smallest size distributions or lowest frequencies where there is significant emission. A test of placing the same temperature cirrus cloud in the two different atmospheres shows that the sensitivity is independent of the underlying atmosphere for higher frequencies or larger size distributions.

The brightness temperature depression depends most strongly on the "average" size of the distribution as indicated by D_m, which is the median of the third power of the particle dimension. There is a factor of 10 in sensitivity between $D_m = 100$ μm and $D_m = 400$ μm. The width of the Gamma distribution has a much smaller effect of, at most, 20% over the range considered here. The range in sensitivity from particle shape is typically a factor of 2 for the same size distribution. Of course, the sensitivity increases dramatically with frequency. The higher frequencies should be able to detect moderate values of cirrus IWP. At 340 GHz for $D_m = 250$ μm an IWP of 60 g m^{-2} generates a nadir brightness temperature depression of 3–6 K depending on shape.

Given the wide range in sensitivities, it is important to be able to infer the average particle size and shape in order to relate a brightness temperature depression to an IWP. Because the sensitivity varies differently with particle size for different frequencies, ratios of brightness temperature depressions at two adjacent frequencies contain information about the size distribution. The most relevant ratio available in this study [$\Delta T_b(340)/\Delta T_b(220)$] is doubled valued; that is, a single ratio can mean either small or large particles, so other information about the size distribution may be needed. If even higher frequencies are used, the ΔT_b frequency ratio becomes less multivalued because more of the size distributions lie on a single branch. Higher frequencies are also more sensitive to cirrus mass and less to the characteristic-particle size.

The ratio of brightness temperature depressions at the two polarizations has information about particle shape. The ΔT_b polarization ratio depends mostly on the particle aspect ratio as well as average size. The probable random attachment of bullets in rosettes complicates the problem of determining their shape from the ΔT_b polarization ratio. The ratio of brightness temperature depressions at the two angles considered here contains information much like the polarization ratio. The range in sensitivity due to particle shape is significantly reduced by using vertical polarization at 49° and expressing the size of the distribution by a characteristic size based on the square of the particle volume.

A specific cirrus microwave remote-sensing algorithm is not presented here because it would depend on the particular experimental setup in question. Instead, some ideas are given for how to use the above results for a remote sensing method. The brightness temperature depression, which is the signal proportional to cirrus IWP, can be found from a brightness temperature image by differencing clear or thin cirrus pixels from the thicker cirrus pixels. Information about average particle size can come from ΔT_b frequencies ratios or from multichannel infrared retrievals. Information about particle shape might be obtained from ΔT_b polarization ratios or assumptions using environmental conditions, such as temperature. Having the size and shape information allows one to use the correct sensitivity to convert the measured brightness temperature to cirrus IWP.

Microwave radiometry will not provide information on the vertical structure of cirrus clouds but should be able to measure integrated properties, such as ice mass and characteristic particle size. Since cirrus clouds are optically thin at microwave frequencies, radiative transfer is linear, and the brightness temperature depression for spatial inhomogeneities or particle mixtures is simply the appropriate average. The effects of cirrus particle shape can be modeled accurately at microwave wavelengths (using the discrete dipole approximation), unlike at the shorter wavelengths in the infrared and visible. The scattering-based microwave method of cirrus retrieval has properties, such as cloud temperature independence, that are different from the emission-based infrared methods. The microwave cirrus retrieval approach is complementary to, and perhaps best used in conjunction with, the window infrared emission and near IR reflectance techniques.

The first microwave instrument appropriate for remote sensing of cirrus is NASA's new MIR (Gasiewski 1992). The MIR is a cross-track scanning instrument

that is mounted on the ER-2. It has total power channels at 89, 150, 183 ± 1, 3, 7, 220, and 325 ± 1, 3, 9 GHz, so only a single polarization (which varies with scan angle) is available. The MIR flew during TOGA COARE in the west Pacific in 1993 but without the 325-GHz channels. The advantages of polarization and even higher frequencies will have to wait for new instrumentation. Future work will include the modeling of more realistic particle shapes and orientations at frequencies beyond 300 GHz and helping to define desirable characteristics for new submillimeter wave radiometers. The results and ideas expressed in this paper, along with radiometer data from the field, should help in the development of cirrus remote-sensing methods for the MIR and future submillimeter wave radiometers.

Acknowledgments. Financial support for this research was provided in part by NASA Grant NAG-5-1592S and NSF Grant ATM-9100795.

REFERENCES

Evans, K. F., and G. L. Stephens, 1991: A new polarized atmospheric radiative transfer model. *J. Quant. Spectros., Radiat. Transfer,* **46,** 412–423.

——, and ——, 1993: Microwave remote sensing algorithms for cirrus clouds and precipitation. Dept. of Atmospheric Science Tech. Rep. 540, Colorado State University, Fort Collins, CO, 198 pp.

——, and ——, 1995: Microwave radiative transfer through clouds composed of realistically shaped ice crystals. Part I: Single scattering properties. *J. Atmos. Sci.,* **52,** 2041–2057.

Fowler, L. D., D. A. Randall, and S. A. Rutledge, 1994: Liquid and ice cloud microphysics in the CSU General Circulation Model. Part I: Model description and simulated microphysical processes. *J. Climate,* submitted.

Gasiewski, A. J., 1992: Numerical sensitivity analysis of passive EHF and SMMW channels to tropospheric water vapor, clouds, and precipitation. *IEEE Trans. Geosci. Remote Sens.,* **30,** 859–870.

Liebe, H. J., G. A. Hufford, and M. G. Cotton, 1993: Propagation modeling of moist air and suspended water/ice particles at frequencies below 1000 GHz. Atmospheric propagation effects through natural and man-made obscurants for visible to mm-wave radiation. *AGARD Conf. Proc.,* **542,** 3.1–3.10.

Liou, K.-N., 1986: Influence of cirrus clouds on weather and climate processes. *Mon. Wea. Rev.,* **114,** 1167–1199.

Ou, S. C., K.-N. Liou, W. M. Gooch, and Y. Takano, 1993: Remote sensing of cirrus cloud parameters using advanced very-high-resolution radiometer 3.7- and 10.9-μm channels. *Appl. Opt.,* **32,** 2171–2180.

Parol, F., J. C. Buriez, G. Rogniez, and Y. Fouquart, 1991: Information content of AVHRR channels 4 and 5 with respect to the effective radius of cirrus cloud particles. *J. Appl. Meteor.,* **30,** 973–984.

Ramanathan, V., and W. Collins, 1991: Thermodynamic regulation of the ocean warming by cirrus clouds deduced from observations of the 1987 El Niño. *Nature,* **351,** 27–32.

Ray, P. S., 1972: Broadband complex refractive indices of ice and water. *Appl. Opt.,* **11,** 1836–1843.

Rossow, W. B., and R. A. Schiffer, 1991: ISSCP cloud data products. *Bull. Amer. Meteor. Soc.,* **72,** 2–20.

Sassen, K., and B. S. Cho, 1992: Subvisual-thin cirrus lidar dataset for satellite verification and climatological research. *J. Appl. Meteor.,* **31,** 1275–1285.

Smith, R. N. B., 1990: A scheme for predicting layer clouds and their water content in a general circulation model. *Quart. J. Roy. Meteor. Soc.,* **116,** 435–460.

Stephens, G. L., and P. J. Webster, 1981: Clouds and climate: Sensitivity of simple systems. *J. Atmos. Sci.,* **38,** 235–247.

Wielicki, B. A., J. T. Suttles, A. J. Heymsfield, R. M. Welch, J. D. Spinhirne, M.-L. C. Wu, D. O. Starr, L. Parker, and R. F. Arduini, 1990: The 27–28 October 1986 FIRE IFO cirrus case study: Comparison of radiative transfer theory with observations by satellite and aircraft. *Mon. Wea. Rev.,* **118,** 2356–2376.

Wiscombe, W. J., 1976: Extension of the doubling method to inhomogeneous sources. *J. Quant. Spectrosc., Radiat. Transfer,* **16,** 637–658.